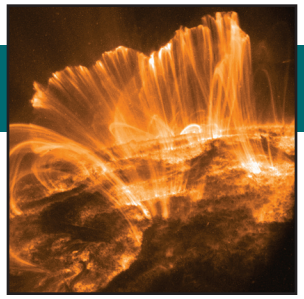

Exploring Solar Flares with Gamma Rays and Neutrons

R. Murphy
Space Science Division

Gamma-ray and neutron emissions from solar flares carry information about the flaring process and conditions within the flaring magnetic loop. Extraction of this information from solar flare measurements requires an ion-acceleration, transport, and interaction model with parameters directly related to those physical processes. In this paper we describe such a magnetic-loop model. Each of the gamma-ray and neutron measurable quantities depends to varying degree on the parameters of the model. We describe these dependences and construct a self-consistent approach to the analysis of high-energy flare data that provides an optimum set of parameters. To illustrate this approach, we summarize the analysis of gamma-ray and neutron data obtained from the 1991 June 4 solar flare with the Oriented Scintillation Spectrometer Experiment (OSSE), a satellite-based instrument developed at NRL.

WHAT ARE SOLAR FLARES AND HOW DO WE LEARN ABOUT THEM?

Solar flares are explosions that occur in the atmosphere of the Sun leading to the emission of radiation covering the full range of the electromagnetic spectrum: radio, visible, UV, X-rays, and gamma rays. The energy released in a solar flare can be greater than 10^{32} ergs, enough to meet the energy demand of the United States for 100,000 years. This enormous amount of energy is dumped into the solar atmosphere in only a few tens of seconds. Flares are often associated with the escape of energetic particles (electrons, neutrons, protons, and heavier nuclei), mass ejections, and shock waves. As the shock waves move through interplanetary space, they also accelerate particles. At Earth, these various phenomena can disrupt radio communication, damage satellites and destabilize their orbits, cause failures in long-distance power lines, change the terrestrial magnetic field, and even endanger astronauts. The potential impact of such solar activity on DoD assets and enterprises is clear.

A solar flare is a stunning, violent, awe-inspiring event occurring on our nearest star, the Sun, an equally awe-inspiring object. What exactly *is* a flare? What is the mechanism that accelerates the energetic particles? How is the energy residing in the Sun's magnetic fields made available for this acceleration? What are the physical conditions at the flaring site and how do they change with time as the flare progresses? What is the connection between the energetic particles directly associated with the flare and the energetic particles seen in interplanetary space? Answering such questions would be reward enough, but with these answers we may be able to predict the occurrence of a flare and its associated disruptions sufficiently early to allow measures to be taken to protect those DoD assets and enterprises.

The frequency of solar flares (along with other aspects of the Sun such as the number of sunspots) varies in an 11-year activity cycle related to the 22-year cycle of the reversal of the Sun's overall magnetic field. As of this writing (early 2008), we are at an activity minimum. This can be seen in Fig. 1, which shows the number of sunspots during the decay after the last activity maximum and predictions for the onset of the next. Surprisingly, some of the largest flares of previous cycles have occurred during the rising portions of the curves, before the maxima had been reached.

Because placing detectors in the hot flaring plasma at the Sun is impossible, solar flares can only be studied remotely via the various emissions they produce. The most easily observed component of flare emission is thermal radiation emitted by the hot plasma. But once the flare energy has been thermalized, most of the information about its initial release and about the subsequent physical processes associated with it are lost. Such information can be better obtained by studying the higher-energy X-ray and gamma-ray emissions produced when the electrons and ions directly accelerated by the energy release subsequently interact with the solar atmosphere. Flares can accelerate electrons to greater than 10 MeV and ions to greater than 1 GeV, corresponding to velocities very near the speed of light. By using such measurements, we seek to learn what specific acceleration process (or processes) is at work and what the physical conditions of the plasma are at the flare site.

Report Documentation Page

Form Approved
OMB No. 0704-0188

1. REPORT DATE	2. REPORT TYPE	3. DATES COVERED
2008		**00-00-2008 to 00-00-2008**

4. TITLE AND SUBTITLE	5a. CONTRACT NUMBER
Exploring Solar Flares with Gamma Rays and Neutrons	5b. GRANT NUMBER
	5c. PROGRAM ELEMENT NUMBER
6. AUTHOR(S)	5d. PROJECT NUMBER
	5e. TASK NUMBER
	5f. WORK UNIT NUMBER
7. PERFORMING ORGANIZATION NAME(S) AND ADDRESS(ES) **Naval Research Laboratory,4555 Overlook Avenue SW,Washington,DC,20375**	8. PERFORMING ORGANIZATION REPORT NUMBER
9. SPONSORING/MONITORING AGENCY NAME(S) AND ADDRESS(ES)	10. SPONSOR/MONITOR'S ACRONYM(S)
	11. SPONSOR/MONITOR'S REPORT NUMBER(S)

12. DISTRIBUTION/AVAILABILITY STATEMENT
Approved for public release; distribution unlimited

13. SUPPLEMENTARY NOTES

14. ABSTRACT

15. SUBJECT TERMS

16. SECURITY CLASSIFICATION OF:			17. LIMITATION OF ABSTRACT	18. NUMBER OF PAGES	19a. NAME OF RESPONSIBLE PERSON
a. REPORT	b. ABSTRACT	c. THIS PAGE			
unclassified	**unclassified**	**unclassified**	**Same as Report (SAR)**	**12**	

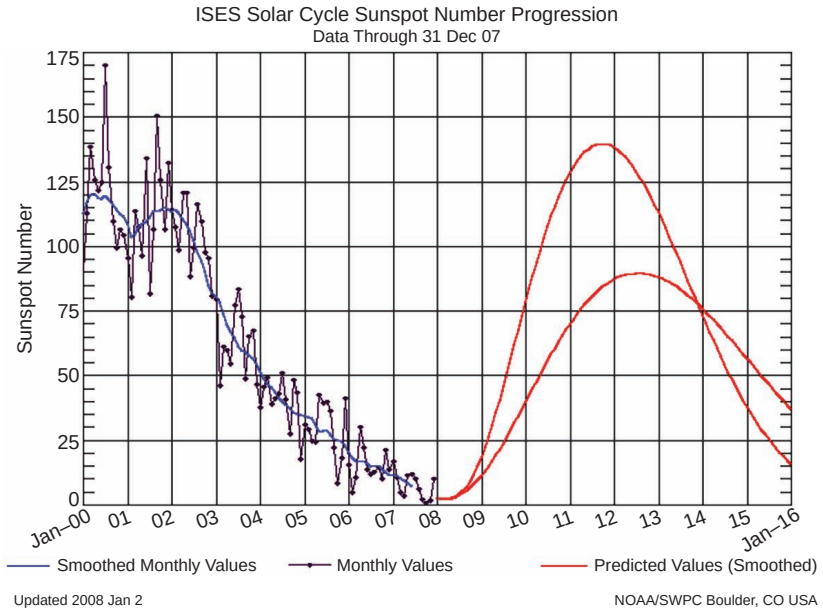

FIGURE 1
Recent sunspot numbers (2000–2007) and predictions for the next activity cycle (2008–2016).

Because X-ray and gamma-ray emissions are easily absorbed by the Earth's atmosphere, their detection requires flying instruments on high-altitude balloons or on satellites, such as the Oriented Scintillation Spectrometer Experiment (OSSE), the Solar Maximum Mission (SMM), the Reuven Ramaty High Energy Solar Spectroscopic Imager (RHESSI), and the Gamma Ray Large Area Space Telescope (GLAST). Such instruments allow the detailed study of flare photon spectra, bringing the power of spectroscopic analysis, a well-known, powerful tool at other wavelengths, to the study of gamma-ray emission from solar flares.

OSSE was designed and built at NRL and launched on NASA's Compton Gamma Ray Observatory (CGRO) in April 1991. Figure 2 shows CGRO being deployed into orbit by the space shuttle *Atlantis*. While its primary scientific goal was celestial, OSSE accomplished excellent observations of a number of solar flares. OSSE provided photon energy spectra from 50 keV to 10 MeV, and detection of gamma rays and neutrons above 10 MeV extended its ability to study solar flares. CGRO was de-orbited in June 2000. The SMM Gamma-Ray Spectrometer was designed and developed as a collaborative effort between the University of New Hampshire, the Max Planck Institute in Garching, Germany, and NRL. The instrument was designed to observe solar X-rays and gamma rays from 10 keV to 100 MeV; it maintained excellent performance throughout its mission from 1980 to 1989. SMM made significant contributions to both solar and celestial astronomy. RHESSI was designed and is operated by the Space Sciences Laboratory at the University of California at Berkeley. Launched in February 2002, RHESSI provides high-resolution spectroscopy and imaging of solar flares from about 3 keV to about 20 MeV. RHESSI is expected to operate throughout the onset of the next activity cycle. GLAST, launched in June 2008, is the next-generation high-energy gamma-ray observatory covering the photon energy range from 10 keV to more than 100 GeV. NRL was responsible for the design and development of the GLAST calorimeter. Intended for making observations of celestial gamma-ray sources, GLAST will also have excellent solar-flare capabilities.

HOW DOES THE ENERGY-RELEASE PROCESS REVEAL ITSELF?

The energy source for particle acceleration in solar flares is undoubtedly related to reconnection of magnetic fields in the corona, the low-density upper atmosphere of the Sun. The Sun's atmosphere is usually divided into three layers. The deepest and most dense layer is the 300-km-thick photosphere, which forms the visible "surface" of the Sun. The temperature of the photosphere decreases from about 6000 degrees Kelvin (K) at its bottom to a minimum of about 4000 K at its top. Above the photosphere is the chromosphere, with a thickness of about 10,000 km. The chromosphere is hotter than the photosphere, extending from the minimum of 4000 K to about 20,000 K where there is an abrupt change to the very hot corona (the region of this abrupt change is called the transition region). The corona extends millions of kilometers into space with temperatures exceeding a million degrees Kelvin.

Magnetic fields dominate the physical processes in the corona, and the field loop structures can be revealed by the bright, hot plasma trapped within them. This is shown by the Transition Region and Coronal Explorer (TRACE) image in Fig. 3(a) obtained at 171 Å, a wave-

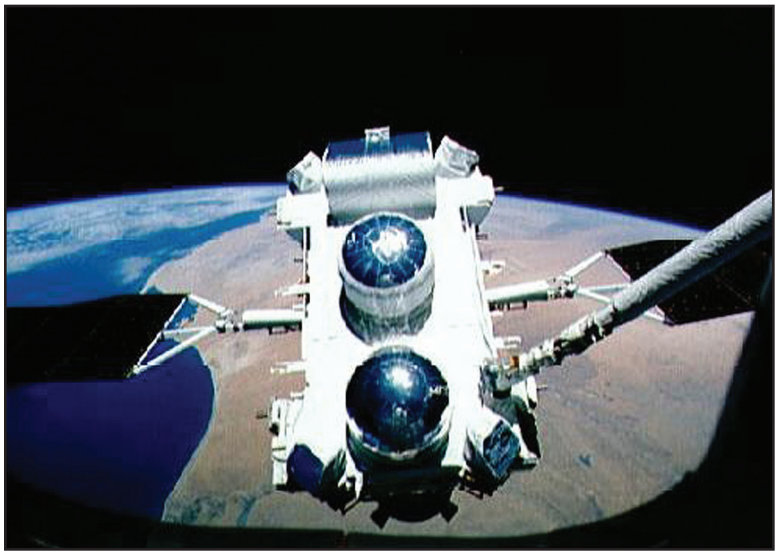

FIGURE 2
Deployment of the Compton Gamma Ray Observatory.

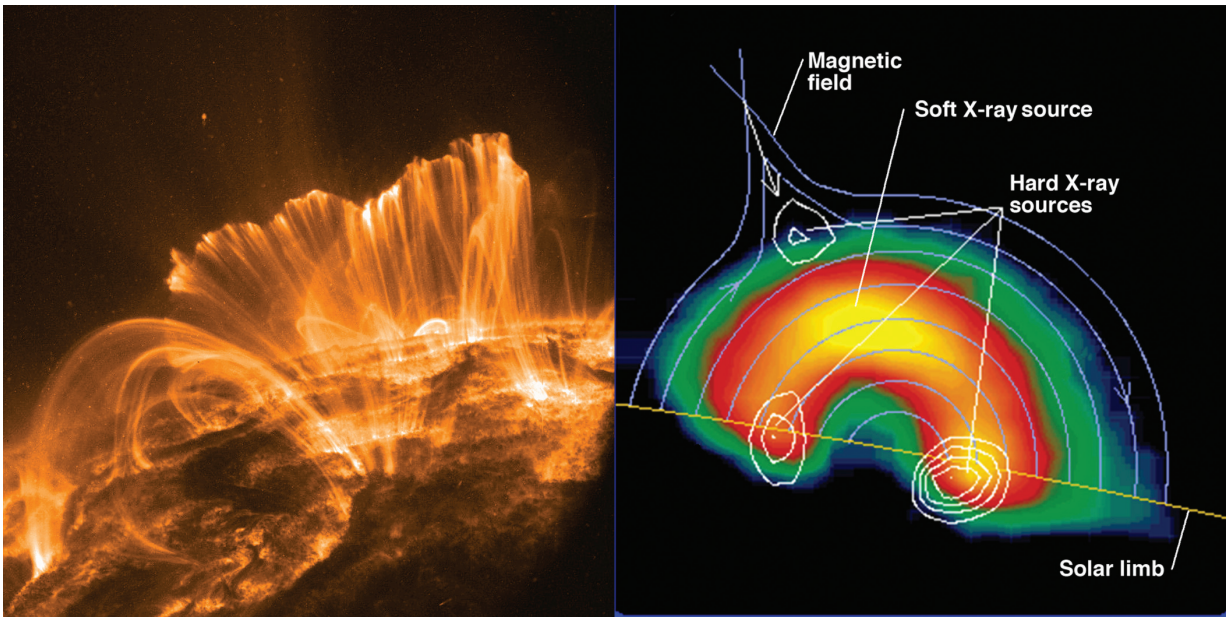

(a) (b)

FIGURE 3
(a) TRACE image (171 Å) of magnetic loops. (b) Yohkoh image of soft X-ray loop and hard X-ray footpoint and looptop emission.

length of light corresponding to a plasma temperature of about a million degrees Kelvin. Images of solar-flare X-ray emission show that such higher-energy emission is concentrated at the footpoints of magnetic loops (see Fig. 3(b)), implying that once the energetic particles are accelerated they are essentially trapped within a loop and interact at the higher densities associated with the footpoints. Acceleration probably occurs near the top of the loop where the density and the associated energy losses are lower, allowing for efficient acceleration. X-ray images of some flares (see Fig. 3(b)) show a third source of emission near the top of loops which may be associated with the acceleration process.

When flare-accelerated electrons interact with the solar atmosphere, they directly produce X- and gamma-ray continuum emission via bremsstrahlung, radiation that occurs when electrically charged electrons are deflected as they pass near electrically charged ambient nuclei. On the other hand, flare-accelerated ions undergo nuclear interactions with the ambient nuclei to produce excited and radioactive nuclei, neutrons, and pions (unstable elementary particles). Some of the neutrons can escape the Sun, but the other products remain trapped in the solar atmosphere and reveal themselves by subsequently producing observable gamma-ray emission via secondary processes. Except for the positron annihilation line (discussed below), gamma-ray emission from accelerated ions arises from nuclear interactions and so does not depend on the temperature or density of the ambient medium, freeing its interpretation from many of the uncertainties associated with atomic-line spectroscopy.

The measurable quantities associated with these various emissions (discussed in the following sections) allow us to learn about the flare process. They convey information about the accelerated ions responsible for their production and also about the physical conditions of the magnetic flare loop in which the particles transport from the acceleration site to the interaction region. Analyses of high-energy solar-flare emissions therefore offer the potential to learn about the structure and evolution of the flare environment in addition to particle acceleration.

Nuclear Deexcitation

An accelerated-ion interaction (for example, an accelerated proton interacting with ambient carbon) can produce a nucleus in one of its excited states which then promptly deexcites (for most nuclei, the lifetimes of excited states are less than 10^{-10} s). The transition produces a photon with energy equal to the energy difference between the two states. As this process is repeated during the course of a flare, gamma-ray lines at specific energies become visible in the spectrum.[1] Most deexcitation-line energies are from 1 to 8 MeV; an example is the 4.439 MeV line that results when a carbon nucleus returns from its first excited state back to its ground state. Motivated by the early detection of solar-flare gamma-ray lines, the cross sections for production of the strongest deexcitation lines from solar flares were measured in the laboratory. Because these cross sections typically peak at a few tens of MeV, deexcitation lines are mostly produced when protons with energies from a few to about 20 MeV interact with ambient solar material.

Because the lifetimes of the excited states are so short, the recoiling nuclei do not lose appreciable energy before they deexcite, and so retain information about the energy and direction of the ion before interaction. This "memory" is then reflected by the precise energy of the emitted photon because it is Doppler-shifted from its rest energy. Studies of the line shapes that result from these Doppler shifts can therefore determine the angular distribution of the accelerated ions when they interacted to produce the excited nuclei. Lines resulting from interactions of the accelerated low-mass protons and alpha (α) particles with ambient nuclei heavier than He are "narrow" (with fractional widths of about 2% of the line energy) because the relatively low recoil velocity of the heavy nucleus results in minimal Doppler shifting of the photons. Heavy accelerated ions interacting with ambient H and He produce "broad" lines (with fractional widths of about 20%) because the heavy nucleus retains much of its initial velocity resulting in significant Doppler shifting.

The measurable quantities associated with deexcitation lines are (1) the time history of the emission, (2) the detailed shape and Doppler shift of the line, and (3) the relative yields of the various lines compared with other emissions. An example of a solar-flare gamma-ray count spectrum is shown in Fig. 4, the 1991 June 4 flare observed with OSSE. The nuclei responsible for the strongest deexcitation lines are noted. There are several lines from the most abundant elements in the solar atmosphere that potentially can be used in flare analyses. Also shown are the various components as determined by fitting the observed spectrum with spectra calculated with a numerical model: the narrow (red) and broad (green) deexcitation lines, and the electron bremsstrahlung (blue). Also shown are the neutron-capture line (dotted) and the positron (e^+) annihilation line (orange), discussed below.

Radioactive Nuclei and the Positron-Annihilation Line

Accelerated-ion interactions also create radioactive nuclei which decay into "daughter" nuclei according to their half-lives, which vary from fractions of a second to days. The decay product can be created in an excited state which again decays promptly, but the

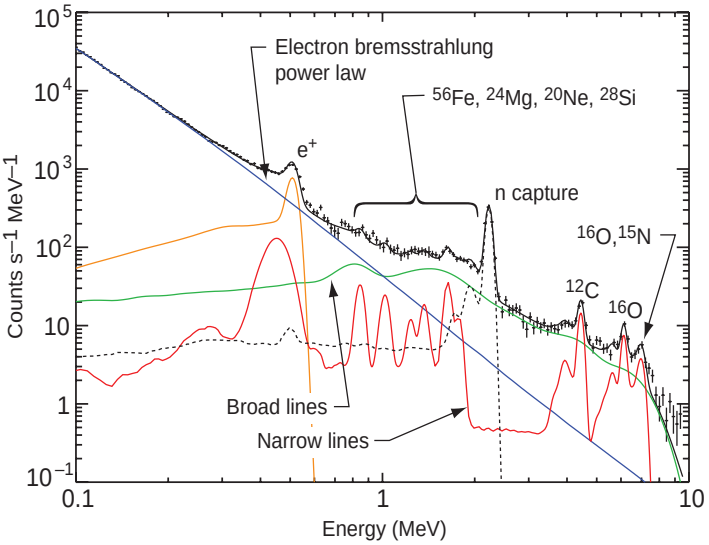

FIGURE 4
Solar-flare gamma-ray count spectrum of the 1991 June 4 solar flare observed with CGRO/OSSE.

appearance of the photon is still delayed relative to the initial nuclear reaction due to the radioactive half-life. Because they are delayed, the detectability of these lines may be enhanced since they appear after the bulk of the prompt emission has decayed away. They are also unique in that they are generally emitted after the recoil radioactive nucleus has had time to slow to thermal speeds, resulting in minimal Doppler shifting and a very narrow line. Because radioactive nuclei usually result from spallation reactions that break the target nuclei apart, their production cross sections generally have thresholds higher than those for deexcitation lines. The accelerated-ion energies are therefore somewhat higher. The measurable quantities associated with line production from radioactive nuclei are (1) the time history of the emission and (2) the yields of the various lines compared with the other emissions.

Many radioactive nuclei decay with the emission of a positron. The initial energies of the positrons are typically several hundred keV, much higher than the thermal energies of the ambient particles. The positrons then lose energy and eventually annihilate with electrons (both free electrons and bound electrons if any partially ionized atoms are present), either directly or through the formation of positronium (Ps), a bound electron-positron "atom." Direct annihilation of a positron-electron pair at rest yields two photons, each of energy 511 keV (the rest mass of an electron or positron), producing a spectral line at 511 keV (see Fig. 4). If positronium is formed, the annihilation depends on the total spin wave function of the Ps and can result in either two 511 keV photons, producing a spectral line at 511 keV, or three photons with energies less than 511 keV, producing a continuum spectrum.

The annihilation process is complex, with the details depending strongly on the temperature, density, and ionization state of the ambient medium. These details determine the shape of the resulting annihilation line and the line/continuum ratio. The positron-annihilation line can therefore be used to probe the ambient conditions at the Sun where the positrons are annihilating. The annihilation line is unique in this, differing from deexcitation lines which, because they result directly from nuclear interactions, are independent of such ambient conditions. At 511 keV, the line energy is significantly lower than most of the deexcitation lines and is more easily scattered as the photons escape through the solar atmosphere, attenuating the line. The measurable quantities associated with the annihilation line are (1) the time history of the emission, (2) the detailed shape of the line, (3) the ratio of the line and Ps continuum yields, and (4) the yield of the line compared with the other emissions.

Neutrons

Ion interactions also produce neutrons which can be observed both directly and indirectly. Because neutrons are uncharged, those initially moving up can escape from the Sun and, if they survive the transit to Earth (neutrons free of the nucleus have a half-life of about 10 minutes), can be directly detected with instruments in orbit. Events with high-energy neutrons >200 MeV can even be detected by monitors on the Earth's surface.

Neutrons initially moving down into the Sun may be indirectly detected because they can be captured on ambient hydrogen to produce deuterium with its

binding energy appearing as a strong gamma-ray line at 2.223 MeV (see Fig. 4). The captures occur deep in the photosphere where the density is high enough so that the time required to be captured is significantly less than the neutron lifetime. Since the probability for elastic scattering is much larger than the probability for capture, most of the neutrons thermalize first, producing a very narrow line and causing a delay in the formation of the capture photon relative to neutron formation. The ambient ^{3}He/H ratio has a strong effect on both the neutron-capture line yield and its delay because non-radiative reactions with ^{3}He compete with the line-producing captures on H.

The yields of the neutron-capture line and the escaping neutrons depend strongly on the angular distribution of the neutrons which in turn depends on the angular distribution of the interacting ions. Neutron production involves interacting-ion energies somewhat higher than those producing excited or radioactive nuclei, extending to 100 MeV. Escaping neutrons surviving to Earth are produced by even higher-energy ions, more than several hundred MeV. The measurable quantities associated with neutron production are (1) the time history of the neutron-capture line, (2) the time-dependent energy spectra of the neutrons arriving at the Earth, and (3) the neutron and neutron-capture line yields compared to the other emissions.

Pions

Neutral and charged pions are mesons produced in interactions of the highest-energy ions (at hundreds of MeV). Neutral pions decay (mean lifetime of 2.6×10^{-8} s) directly into two 67.5 MeV gamma rays. Charged pions decay (mean lifetime of 0.84×10^{-16} s) via muons into positrons and electrons which produce bremsstrahlung gamma rays. Positrons from positively charged pions also produce annihilation radiation, both continuum when the decay positrons annihilate in flight and 511 keV line emission when they annihilate near rest. Because the high-energy ions that produce pions can penetrate deep into the solar atmosphere, the low-energy annihilation photons will be scattered escaping the Sun, attenuating the line. The measurable quantities associated with pion-decay emission are (1) the time history of the emission, (2) the spectral shape of the radiation, and (3) its yield compared to the other emissions.

HOW IS INFORMATION EXTRACTED FROM SOLAR FLARE MEASUREMENTS?

A model is typically required to understand a complex physical system and to make predictions of its behavior, with the model described by a set of parameters representing the properties of the system. A solar flare is a very complex system and to extract information about the flare process from high-energy flare measurements, we have developed a flare-loop transport and interaction model. The model incorporates those aspects of transport and interaction of flare-accelerated ions in a loop that are most important for gamma-ray and neutron production. It reflects the evolution of our understanding of the flare process over several decades since the foundations of high-energy flare interactions were established in a series of papers by R. Ramaty, R. Lingenfelter, and B. Kozlovsky. The energy- and angle-dependent cross sections for the most important nuclear reactions in solar flares have been measured in the laboratory. Information about the remaining reactions has been obtained with theoretical nuclear-reaction computer codes such as TALYS.

The magnetic-loop model is represented by a group of computer codes and is described by a set of parameters (discussed below) related directly to the physical processes and conditions at the flare site. For a given set of choices for these parameters, the model provides expected values for the measurable quantities associated with gamma rays and neutrons, which can be compared with observations. The parameter values may then be adjusted to give the best agreement of prediction with measurement among all the measurable quantities. But because many of the measurable quantities depend on the same parameters, deriving well-constrained values for those parameters is challenging. Early analyses often did not take these complicated inter-dependences into account in a systematic way, addressing only a limited number of parameters.

With the flare-loop model, all of these inter-dependences can be systematically addressed by identifying all relevant parameters, showing how the nature of the nuclear interactions depend on them and how the various measurable quantities are subsequently affected. With this understanding, we have constructed a comprehensive, self-consistent approach to the analysis of flare data. Success of the approach, however, does require that the available flare measurements cover a sufficiently broad range of the measurable quantities.

The Flare-Loop Transport and Interaction Model

Figure 5(a) shows a schematic diagram of a flaring loop, directly reflecting the flare-loop geometry as observed (compare with Fig. 3(b)). Figure 5(b) shows the corresponding flare loop model. The model consists of a semicircular coronal portion of length L and two straight portions extending vertically from the transition region through the chromosphere into the photosphere. Below the transition region, the magnetic field strength $\mathbf{B}$ is assumed proportional to a power δ of the pressure. Such a converging magnetic field can result in mirroring of accelerated particles. Turbulence in

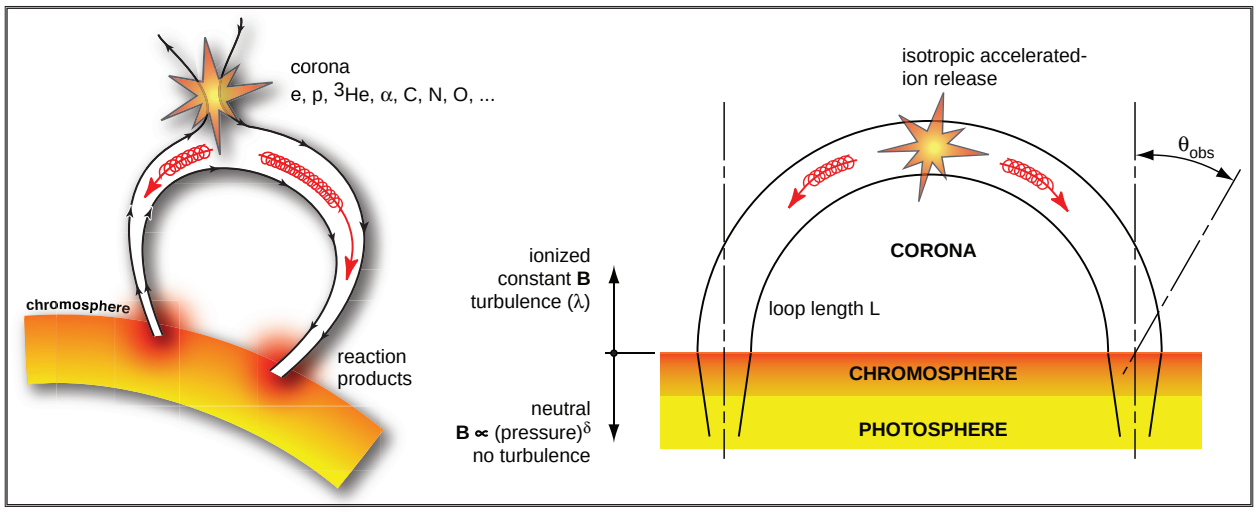

FIGURE 5
(a) flare loop schematic; (b) loop model.

the loop can cause pitch-angle scattering (PAS) which is characterized by λ, the mean free path required for an arbitrary initial angular distribution to relax to an isotropic distribution. We assume a particular density height profile $n(h)$ and ambient elemental composition for the solar atmosphere. Accelerated ions are released isotropically at the top of the loop with an assumed elemental composition and kinetic-energy spectrum (typically, a power law in energy with index s). The heliocentric angle of the flare site on the solar disc, θ_{obs}, is the angle between the normal to the solar surface at the flare and the direction to the Earth.

Using this model we have explored the dependence of the measurable quantities on the parameters. The properties of an interacting accelerated ion that most significantly affect the properties of the subsequent gamma-ray and neutron emissions are (1) the time of the interaction after release from the acceleration region, (2) the ion direction of motion at interaction, and (3) the ion kinetic energy at interaction.

Interaction Time Scale

In the absence of magnetic convergence ($\delta = 0$), ions do not mirror and the nuclear interaction time history depends only on the transit time down the loop (which depends on the loop length L) and the energy loss rate in the atmosphere (which depends on the density n). In the presence of magnetic convergence ($\delta \neq 0$), ions with initial pitch angles lying close to the loop axis also do not mirror (they are within the "loss cone") and behave similarly. Ions outside the loss cone mirror and lose energy much more slowly as they repeatedly traverse the low-density corona. Interactions of these ions thus occur on longer time scales, with the time scale increasing with increasing convergence δ. Turbulence in the loop causes particles to be scattered into the loss cone, continuously repopulating it. As a result, with more scattering (smaller λ) the nuclear interaction rate increases at early times and correspondingly decreases at later times.

Interacting-Ion Angular Distribution

In the absence of magnetic convergence ($\delta = 0$), there is no mirroring and the angular distribution of the interacting ions will be downward isotropic regardless of the level of PAS. In the presence of magnetic convergence ($\delta \neq 0$) but no PAS, most ions mirror and the interactions occur mostly at the ion mirror points where the density is greatest. Thus, most ions are moving parallel to the solar surface when they interact, in a "fan beam" angular distribution. Any downward contribution from those ions that do not mirror becomes even less important as δ increases. By continuously repopulating the loss cone, the effect of PAS is to produce more interactions involving downward-directed ions. This can be seen in Fig. 6, showing angular distributions for a moderate amount of magnetic convergence ($\delta = 0.2$) and three levels of PAS. Here, $\mu = \cos(\theta)$ where θ is the angle between the normal to the solar surface and the direction of the ion. With no PAS, the distribution is peaked at $\theta = 90°$ ($\mu = 0$), a fan-beam distribution, with some downward-directed interactions ($\mu < 0$) from ions originally in the loss cone. As PAS increases (λ decreases), the distribution becomes more downward directed. A consequence of the angular distribution is that when it is more downward-directed, the interactions occur deeper in the solar atmosphere.

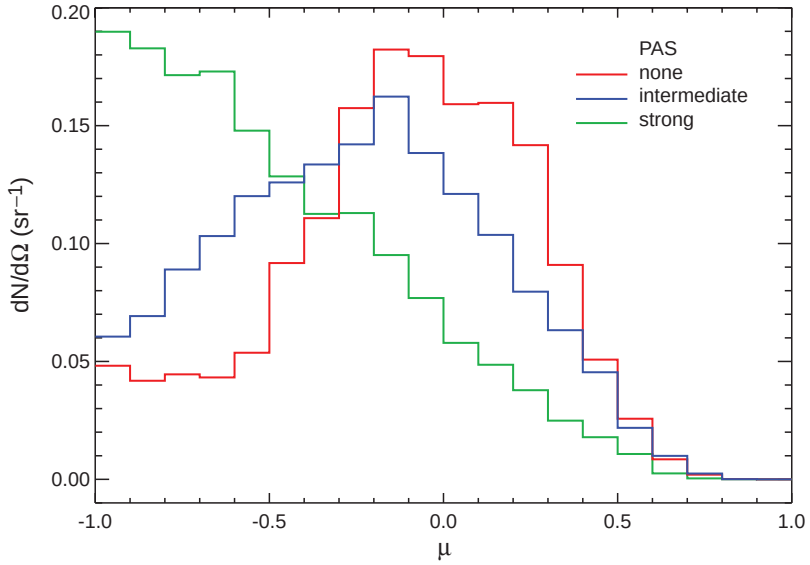

FIGURE 6
Angular distribution (reactions per steradian) of the interacting ions for δ = 0.2 and several values of pitch angle scattering (PAS).

Ion Energy at Interaction

The energies of the accelerated ions at interaction are mostly determined by the combination of the accelerated-ion spectral steepnesss (steeply falling spectra are referred to as "soft" and less steeply falling spectra as "hard") and the ion-energy dependence of the specific production cross section. On average, harder accelerated-ion spectra result in higher interacting-ion energies. However, cross sections involving energetic α particles typically have lower threshold energies, so increasing the ratio of the number of accelerated α particles to protons (α/p) shifts the interacting-ion energies lower.

The Dependence of the Measurable Quantities on the Loop Model Parameters

Table 1 summarizes the measurable quantities and indicates those loop parameters that affect each. In the following we discuss some of the most important of these parameter dependences. We distinguish two types of parameters: (1) acceleration parameters describing aspects of the accelerated ions and (2) physical parameters describing aspects of transport within the loop.

Narrow deexcitation-line yields and ratios depend on (1) the steepness of the accelerated-ion spectrum (here assumed a power law with index *s*) because of the different ion-energy dependences of their line-production cross sections, (2) the ratio of the number of accelerated α particles to protons (α/p) since both species contribute to narrow lines, and, most directly, (3) the relative abundances of the target elements in the solar atmosphere. The shape and Doppler shift of the lines depend on (1) the α/p ratio since the heavier α particles produce higher recoil velocities for the excited nucleus, (2) the ion spectrum since a harder spectrum has more high-energy ions producing higher recoil velocities, and (3) the interacting-ion angular distribution, most directly determined by magnetic convergence (δ) and PAS (λ). Since the interacting-ion angular distribution is typically not isotropic, the location of the flare on the Sun (θ_{obs}) will also affect the observed line shape. The time history will depend on the loop length *L* and on the amount of mirroring (through δ and λ).

The neutron-capture line yield depends on (1) the accelerated-ion spectral index *s*, (2) the α/p ratio, (3) the interacting-ion angular distribution (through δ and λ) since neutrons must be moving downward to be efficiently captured, and (4) the photospheric abundance of ^{3}He. Because the captures occur deep in the photosphere, the capture photons can be strongly scattered, resulting in attenuation of the line, especially for flares near the solar limb where the path-length through the solar atmosphere is large. The flare location θ_{obs} is thus an important parameter. The time history depends on (1) the interacting-ion angular distribution (through δ and λ), (2) the photospheric abundance of ^{3}He, and (3) the flare location θ_{obs}.

Similar to the neutron-capture line, the time- and energy-dependent energy spectra of the neutrons escaping the Sun and arriving at Earth depend on (1) the accelerated-ion spectral index *s*, (2) the α/p ratio, (3) the interacting-ion angular distribution (through δ and λ), (4) the loop length *L*, and (5) the flare location θ_{obs}.

The yield of the annihilation line (which follows from positron production), depends on (1) the accelerated-ion spectral index *s*, (2) the α/p ratio, and, since the line can be more easily scattered than the deexcitation lines, on (3) the depth of the positron production (through δ and λ). Because of this scattering, the yield also depends on (4) the flare location θ_{obs}. The detailed

TABLE 1 — Measurable Quantities of High-Energy Flare Emissions and the Loop Model Parameters that Affect Them

Measurable Quantity	Acceleration Parameter	Physical Parameter
narrow deexcitation line fluences and ratios	α/p, s	ambient abundances
narrow deexcitation line shift and shape	α/p, s	δ, λ, θ_{obs}, $n(h)$
narrow deexcitation line time history	$a_{ion}(t)$	δ, λ, L, $n(h)$
neutron-capture line fluence	α/p, s	δ, λ, θ_{obs}, $n(h)$ ambient ^{3}He/H
neutron-capture line time history	$a_{ion}(t)$, α/p, s	δ, λ, θ_{obs}, L, $n(h)$ ambient ^{3}He/H
neutron fluence at Earth	α/p, s	δ, λ, θ_{obs}, $n(h)$
neutron arrival time history at Earth	$a_{ion}(t)$, α/p, s	δ, λ, θ_{obs}, L, $n(h)$
511 keV line fluence	α/p, s, ^{3}He/^{4}He acc. abundances	δ, λ, θ_{obs}, $n(h)$, T, X ambient abundances
511 keV line shape and continuum	α/p, ^{3}He/^{4}He, s	δ, λ, θ_{obs}, $n(h)$, T, X
511 keV line time history	$a_{ion}(t)$, α/p, s acc. abundances	δ, λ, θ_{obs}, L, $n(h)$, X
pion-decay radiation yield	α/p, s	ambient abundances
pion-decay radiation spectral shape	α/p, s	δ, λ, θ_{obs}, $n(h)$
pion-decay radiation time history	$a_{ion}(t)$	δ, λ, L, $n(h)$
images	—	L, θ_{obs}

shape of the line depends on the annihilation process which, in turn, depends on the density (n), temperature (T), and ionization state (X) of the ambient medium.

The yield and spectral shape of pion-decay radiation depends on (1) the accelerated-ion spectral index s, (2) the α/p ratio, and (3) the interacting-ion angular distribution (through δ and λ).

Analysis Algorithm for Solar-Flare Gamma-Ray and Neutron Data

From Table 1 and the above discussion we see that while there are a large number of quantities that can be measured, there are also a large number of parameters to be determined. In addition, each of the measurable quantities can depend on several parameters. Restricting an analysis to one or a small subset of the measurable quantities can result in parameter estimates that may be inconsistent with estimates derived from analysis of other measurable quantities. And if the effect of all of the relevant parameters are not properly taken into account, the uncertainties can be underestimated. A reliable analysis must utilize as many measurable quantities as possible to determine as many parameters as possible. But because of the many inter-dependences, this can be quite challenging, and additional assumptions may still be required to make progress in constraining the parameters.

We have developed a data-analysis algorithm that provides the approach and analysis steps necessary for a comprehensive analysis of solar-flare gamma-ray line and neutron data.[1,2,3] The guiding principle of the algorithm is to first consider those measurable quantities that depend on only one or two parameters and then, using those parameter estimates, proceed to other measurables that have more complicated dependences. To illustrate the procedure, we summarize some of the results from our recent analysis of the high-energy flare data available for the 1991 June 4 flare observed with OSSE (among other instruments). The June 4 flare remains unique for its breadth of available high-energy emission measurements. In that analysis, we established well-constrained values for the parameters and showed that the loop model can account for the wide variety of measurements available for this flare with reasonable values for the parameters.

In June 1991, an active region rotated onto the solar disk and produced some of the largest flares ever recorded. The active region first appeared at the east limb on June 1 and produced an intense flare. The peak of this flare was missed by the CGRO instruments due to a routine shut-down. As there was a high probability for subsequent intense flares, a solar Target of Opportunity was declared and OSSE stopped observing its current celestial target and re-oriented to the Sun. On June 4, a second intense flare occurred while OSSE was viewing the Sun. The flare was one of the most powerful nuclear gamma-ray line flares observed to date; most instruments, from the soft X-ray to the gamma-ray bands, saturated at its peak. Energetic particles from the flare were observed in interplanetary space by the Ulysses EPAC experiment, GOES, and IMP-8 platforms. In the visible light of Hα, the flare was located at N30E70, corresponding to a heliocentric angle θ_{obs} of about 74°.

We began the analysis with the parameter that is most directly established, the size of the flare loop determined from white-light images of the flare. (Ideally, images of gamma-ray emission loop footpoints, such as obtained with RHESSI for more recent flares, would be used.) We assume the white-light patches in the images to be footpoints where the ions interact, implying loop lengths from 11,500 km to 65,000 km, depending on which pair of patches is assumed to be associated with the loop producing the gamma rays.

The next parameter to be determined was the accelerated α/p ratio. The most direct measure of α/p is the measured fluence ratio of the 0.45 MeV deexcitation-line complex (produced exclusively by accelerated α particles) and a narrow line such as the 4.439 MeV line of C. However, this ratio also depends on the accelerated-ion spectral index s. The spectral index can be determined from the measured fluence ratio of the 6.129 MeV O and 1.634 MeV Ne lines, but this ratio also depends on α/p. We therefore simultaneously determined α/p and s by calculating values of the two fluence ratios for a range of assumed values for α/p and s and comparing them with measured fluence ratios. This provided a confidence region for the two parameters: the accelerated α/p ratio was at least 0.4 (considerably larger that the value of 0.03 found in the corona) and the spectral index s was 3.9 ± 0.2 (similar to the average value of ~4.2 found from analyses of SMM flares).

With α/p and s now determined, we next constrained δ and λ using the measured Doppler shift of the 4.439 MeV C line. Unfortunately, Doppler shifts from flares such as this located nearer the limb than disk center are minimal, and the resulting constraint was not useful. However, combining it with the δ–λ constraint obtained from the time history of deexcitation lines (using our already-determined value for the loop length L), we obtained a well-constrained confidence region for the two parameters. We found that convergence of the magnetic field was required and that turbulence was present in the loop.

Finally, using all of the parameter values determined so far, we calculated neutron spectra arriving at Earth and compared them with neutron count rates

obtained with OSSE. We found that the number of neutrons arriving at Earth was over-predicted, especially at early times. This can be seen in Fig. 7 comparing the measured (data points) and predicted (green curve) neutron count rates. Neutrons arriving early are higher-energy neutrons produced by high-energy accelerated ions. Reducing the number of high-energy neutrons relative to low-energy neutrons can be achieved if the accelerated-particle spectrum steepens with energy, as long as this does not affect the other measurable quantities previously analyzed. This is possible since those emissions are produced by accelerated ions with lower energies than the ions producing the neutrons escaping into space and surviving to Earth. We also show in Fig. 7 (red curve) the predicted neutron arrival time history calculated with a cutoff ion energy E_c = 125 MeV. We confirmed that such a cutoff did not affect the other calculated quantities.

DISCUSSION

This article presents our model for gamma-ray and neutron production by flare-accelerated ions in a magnetic loop, with model parameters directly related to the physical processes and conditions at the flare site. With this model, all of the measurable quantities associated with high-energy flare emission can be calculated, and comparison of model predictions with measurements provides constraints on the parameters. But the dependences of the measurable quantities on the parameters is complex and obtaining parameter constraints can be difficult. We developed a flare-analysis algorithm that allows, for the first time, a comprehensive analysis of all measurable quantities. The algorithm considers first those measurable quantities that depend on only one or two parameters and then, with those parameter estimates, proceeds to other observables that have more complicated dependences. Reliable determination of all of the parameters requires that the observations cover a sufficiently wide range of the measurable quantities. To illustrate the procedure, we summarized our analysis of the 1991 June 4 flare, remarkable for its range of high-energy emission measurements.

The analysis procedure can be applied to other flares having a similarly wide range of measurable quantities, and we look forward to applying it to flare data obtained with GLAST as the new activity cycle develops. With the extended photon-energy range of GLAST, we will be able to expand our studies to the highest accelerated-ion energies. As our understanding of solar flares improves, we will be nearer the goal of predicting solar activity and preventing disruptions in our increasingly technology-dependent lives and endeavors.

ACKNOWLEDGMENTS

This work is built on many years of research by many investigators, including R. Ramaty, B. Kozlovsky, R. Lingenfelter, G.H. Share, and X.-M. Hua.

[Sponsored by NASA and ONR]

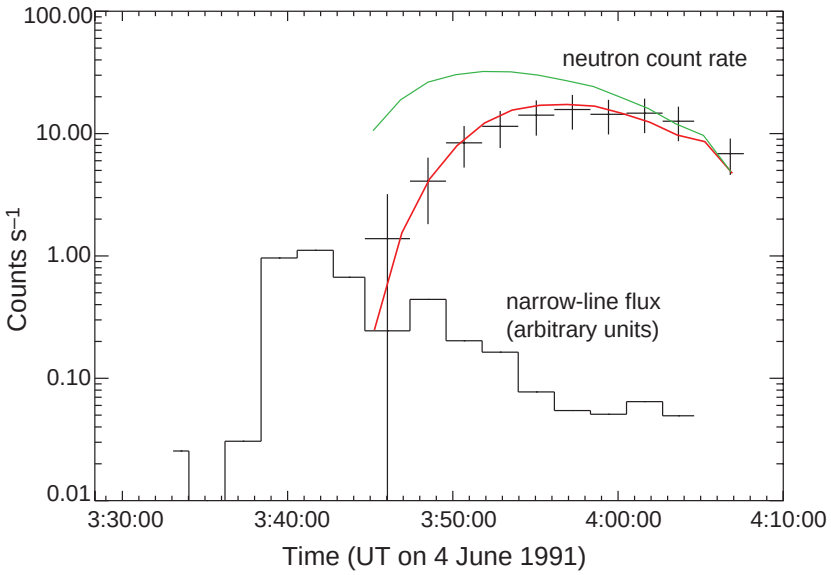

FIGURE 7
Comparison of the neutron count rate time history measured with OSSE from the June 4 flare with calculated count rate time histories. The green curve is for an unbroken power-law accelerated-ion spectrum and the red curve is for a spectrum cut off at E_c = 125 MeV. Also shown is the time history of the narrow deexcitation line flux (histogram).

References

[1] R. Ramaty, B. Kozlovsky, and R.E. Lingenfelter, "Nuclear Gamma-Rays from Energetic Particle Interactions," *Astrophysical Journal Supplement Series* **40**, 487-526 (1979).

[2] B. Kozlovsky, R.J. Murphy, and R. Ramaty, "Nuclear Deexcitation Gamma-Ray Lines from Accelerated Particle Interactions," *Astrophysical Journal Supplement Series* **141**, 523-541 (2002).

[3] R.J. Murphy, B. Kozlovsky, G.H. Share, X.-M. Hua, and R.E. Lingenfelter, "Using Gamma-Ray and Neutron Emission to Determine Solar Flare Accelerated Particle Spectra and Composition and the Conditions within the Flare Magnetic Loop," *Astrophysical Journal Supplement Series* **168**, 167-194 (2007). ★

THE AUTHOR

RON MURPHY received a B.S. in physics in 1979 and a Ph.D. in 1985, both from the University of Maryland. His thesis research involved high-energy emission from solar flares. He came to NRL in 1988 in a joint appointment with NRL and NASA Goddard Space Flight Center, then as a National Research Council researcher, and finally as a civil servant in 1990. He has continued his research involving solar flares, authoring and co-authoring a number of articles in refereed scientific publications. His research involves both theoretical calculations and analysis of gamma-ray and neutron data from a number of satellite instruments.